Mecánica Computacional Vol. XXIII, pp. 45-58
G.Buscaglia, E.Dari, O.Zamonsky (Eds.)
Bariloche, Argentina, November 2004

EXPERIMENTAL AND NUMERICAL CHARACTERIZATION OF DAMAGE EVOLUTION IN STEELS

Diego J. Celentano[*], Patricio E. Tapia[*], and Jean-Louis Chaboche[†]

[*] Departamento de Ingeniería Mecánica
Universidad de Santiago de Chile
Avda. Bdo. O´Higgins 3363 - Santiago de Chile - CHILE
e-mail: dcelenta@lauca.usach.cl

[†] Office National d'Etudes et de Recherches Aérospatiales
ONERA, DMSE
29, Av. de la Division Leclerc, 92320 Chatillon - FRANCE
e-mail: Jean-Louis.Chaboche@onera.fr

Key words: continuum damage mechanics, mechanical characterization.

Abstract. *This paper presents an experimental and numerical characterization of ductile damage evolution in steels subjected to large plastic deformations. To this end, a set of tensile tests combining load-unload cycles is firstly carried out in order to evaluate the deterioration exhibited by the Young's modulus for increasing levels of plastic deformation. This task allows, in turn, to derive the characteristic parameters involved in a well-established evolution equation for the isotropic damage variable. All these material parameters are the basic data to be considered in the simulations that are performed afterwards: the analysis of the tensile test is mainly aimed at assessing the proposed characterization while the modelling of the flattening process of a cylinder is considered to discuss the possibilities and limitations of the constitutive model.*

1 INTRODUCTION

The phenomenon of ductile plastic damage usually refers to the initiation, coalescence and growth of cavities and microcraks induced by large deformations in metals. Its extensive study within the general framework of thermodynamics of irreversible processes led to the development of Continuum Damage Mechanics [1-9]. Different damage definitions and related models have been proposed and used in the last decades [1-12]. The most classical definition of isotropic damage is given by a scalar variable that accounts for the surfacic density of microcraks and cavities in any plane of a representative volume element [5-9].

In general, the damaging processes are reflected in a progressive material deterioration which can be measured through the decrease of strength, stiffness, toughness, etc [1-9]. However, reliable measurements of damage is still nowadays a challenging task. The experimental procedures to estimate the damage evolution in a material subjected to loads can be classified in two main groups: direct and non direct measurements [7]. This last group encompasses, in turn, destructive and non-destructive methods. The main features of these procedures as well as their advantages and drawbacks are detailed in [7].

An experimental and numerical characterization of ductile isotropic damage evolution in steels subjected to large plastic deformations is proposed in this work. To this end, a set of load-unload tensile tests were firstly carried out on cylindrical specimens of SAE 1020 and SAE 1045 steels in order to obtain their stress-strain curves which allow, in turn, to derive their elastic, strain hardening and damage characteristic parameters. Then, the deformation process experienced by these materials during the test is numerically simulated via a large strain isotropic elasto-plastic constitutive model that also accounts in a coupled form for both hardening and damage effects. The corresponding numerical results are validated with the experimental measurements. Finally, the damage evolution during the flattening process of a cylinder is analysed.

2 EXPERIMENTAL PROCEDURE

Among the different possible methods to measure ductile damage evolution in a metal subjected to deformation, a suitable destructive procedure is that related to the variation of the effective elasticity modulus $\widetilde{E}$ due to the appearance of microcracks and cavities inside the material [5-9]. To this end, load-unload tensile tests are needed in order to track the deterioration or degradation of $\widetilde{E}$ reflected, at high levels of deformation, in the slope change in the stress-strain curve corresponding to the elastic response during the unloading or reloading in a cycle. The engineering stress-strain curves obtained for the SAE 1020 and SAE 1045 steels are shown in Figure 1. In this context, the damage variable d^p can be computed for each unload-reload cycle as:

$$d^p = 1 - \frac{\widetilde{E}}{E} \tag{1}$$

where E is the Young's modulus of the undamaged material (usually adopted as that of the

first load path in the tensile test) and $\widetilde{E}$ is, as mentioned above, the effective Young's modulus accounting for damage effects. In this work, $\widetilde{E}$ has been evaluated as an average between the uniaxial moduli corresponding to the unload and reload elastic path of each cycle *i*. Thus,

$$\widetilde{E}_i^{uniaxial} = \frac{\dfrac{P_i^u - P_i^l}{A_i^l}}{\dfrac{L_i^u - L_i^l}{L_i^l}} \tag{2}$$

where *P* is the load, *A* is the current transversal area of the sample (the undeformed one is denoted as A_0), *L* is the current extensometer length and superindexes *u* and *l* respectively refer to the upper and lower points located in the elastic path of the stress-strain curve (see Figure 1). Due to the small deformations involved in the elastic paths, note that $A_i^u \approx A_i^l$ for every cycle. The experimental $\widetilde{E}^{uniaxial} - \ln(A_0 / A)$ measurements are respectively plotted in Figures 3.a and 4.a for the two steels studied in this work. Two straight lines bounding the experimental uncertainty range have been drawn with the sake of dealing with the scattered nature of the data. A third line obtained as their average is also depicted. In what follows, the experimental procedure will take into account these lines in order to characterize the damage response. It is seen that $\widetilde{E}^{uniaxial}$ increases at high levels of deformation. As already pointed out in [5-7], this is due to the triaxial stress state that occurs in the samples after the necking formation that causes, in turn, the decrease of the load. A procedure avoiding this inconvenient is based on strain-gauge measurements performed at low-deformation tension-compression cycles. This methodology, however, is too much complicate since the strain-gauges need to be reinstalled at every load cycle and, besides, the derivation of $\widetilde{E}$ is not straightforward due to the coupling of the normal components existing in the stress-strain law. In order to obtain the real damaged Young's modulus $\widetilde{E}$ from the uniaxial measurements $\widetilde{E}^{uniaxial}$, an alternative procedure is proposed in this work. It is based on the following expression:

$$\widetilde{E} = f_E \, \widetilde{E}^{uniaxial} \tag{3}$$

where f_E is a correction factor that eliminates the triaxial effect inherent to $\widetilde{E}^{uniaxial}$. The methodology followed to derive such a correction factor can be found in [13] and it basically consists in applying equation (2) to the results corresponding to a simulation without damage effects, denoted as $\widetilde{E}^{uniaxial-wd}$, in such a way that the correction factor can be computed by the following relationship $f_E = E / \widetilde{E}^{uniaxial-wd}$. The f_E-$ln(A_0/A)$ relationships for both steels are shown in Figure 2. The real Young's modulus versus logarithmic strain curves obtained by applying equation (3) to the two outer lines of Figure 3.a and 4.a are respectively plotted in Figures 3.b and 4.b. As expected, the real Young's modulus exhibits a decreasing trend for large strain values. Finally, the damage curves in terms of the logarithmic deformation

computed via equation (1) with the data provided by Figures 3.b and 4.b are respectively shown in Figures 3.c and 3.b. These last curves allow to derive three parameters that, according to [5-9], are assumed to characterize the material damage response in a monotonically loaded uniaxial tensile by means of:

$$d^{p} = \frac{d_r}{(\bar{e}_r - \bar{e}_d)} \left\langle \bar{e}^{p} - \bar{e}_d \right\rangle \tag{4}$$

where d_r is the critical damage value found at the failure strain $\bar{e}_r$, $\bar{e}_d$ is the so-called damage threshold, $\bar{e}^p$ is the effective plastic strain whose evolution will be detailed in Section 3 and $\langle\ \rangle$ are the Macauley brackets (i.e., $\langle x \rangle = x$ if x>0 and $\langle x \rangle = 0$ otherwise). The experimentally measured average values for $\bar{e}_d$, $\bar{e}_r$ and d_c are listed in Table 1. This is the basic data considered in the simulations shown in Section 4.

3 GOVERNING EQUATIONS AND CONSTITUTIVE MODEL

The evolution of an assumed quasi-static process (i.e., that with negligible inertia effects and identically fulfilled energy balance) can be described by local governing equations expressed by the mass conservation, linear momentum balance and the dissipation inequality (all of them valid in $\Omega x \Upsilon$, where Ω is the spatial configuration of a body and Υ denotes the time interval of interest with $t \in \Upsilon$) respectively written in a Lagrangian description as [14]:

$$\rho J = \rho_0 \tag{5}$$

$$\nabla \cdot \boldsymbol{\sigma} + \rho \mathbf{b}_f = \mathbf{0} \tag{6}$$

$$D_{\text{int}} \geq 0 \tag{7}$$

together with appropriate boundary conditions and an adequate constitutive relation for the Cauchy stress tensor $\boldsymbol{\sigma}$ (which is symmetric for the non polar case adopted in this work). In these equations, ρ is the density, J is the determinant of the deformation gradient tensor $\mathbf{F}$ ($\mathbf{F}^{-1} = \mathbf{1} - \nabla \mathbf{u}$, where $\mathbf{1}$ is the unity tensor, ∇ is the spatial gradient operator and $\mathbf{u}$ is the displacement vector), the subscript *0* applied to a variable denotes its value at the initial configuration Ω_0, $\mathbf{b}_f$ is the specific body force vector and D_{int} is the internal dissipation which imposes restrictions over the constitutive model definition. In this framework, a specific Helmholtz free energy function ψ, assumed to describe the material behavior during the deformation process, can be defined in terms of some thermodynamic state variables chosen in this work as the Almansi strain tensor $\mathbf{e}$ ($\mathbf{e} = 1/2(\mathbf{1} - \mathbf{F}^{-T} \cdot \mathbf{F}^{-1})$, where T is the transpose symbol) and a set of n_{int} phenomenological internal variables α_k (usually governed by rate equations with zero initial conditions and $k = 1,...,n_{\text{int}}$) accounting for the non-reversible effects [1-15]. This free energy definition, is only valid for small elastic strains and isotropic

material response, both assumptions being normally accepted for metals and other materials. Invoking the Coleman's method [15], the following relationships are obtained: $\boldsymbol{\sigma} = \rho \partial\psi / \partial \mathbf{e}$ and $D_{\text{int}} = \mathbf{q}_k * D\boldsymbol{\alpha}_k / Dt$ where $\mathbf{q}_k = -\rho_0 \partial\psi / \partial \boldsymbol{\alpha}_k$ are the conjugate variables of $\boldsymbol{\alpha}_k$ and, according to the nature of each internal variable, the symbols $*$ and $D(\cdot)/Dt$ appearing in the previous expressions respectively indicate an appropriate multiplication and a time derivative satisfying the principle of material frame-indifference [15].

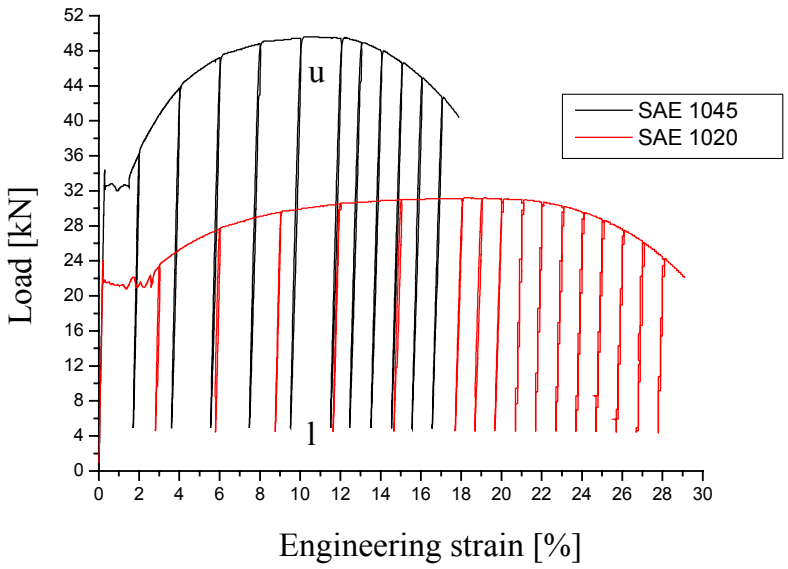

Figure 1: Engineering stress-strain curves for SAE 1020 and SAE 1045 steels.

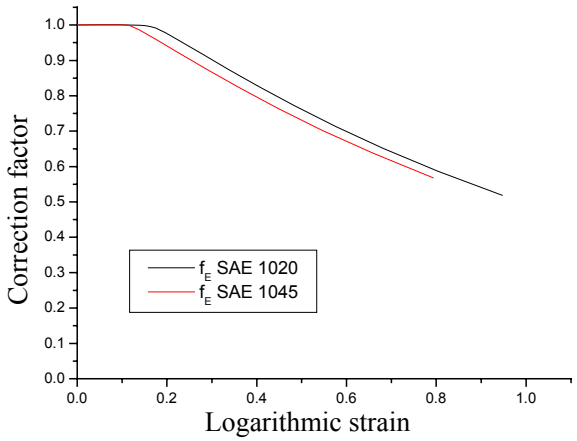

Figure 2: Correction factors for SAE 1020 and SAE 1045 steels.

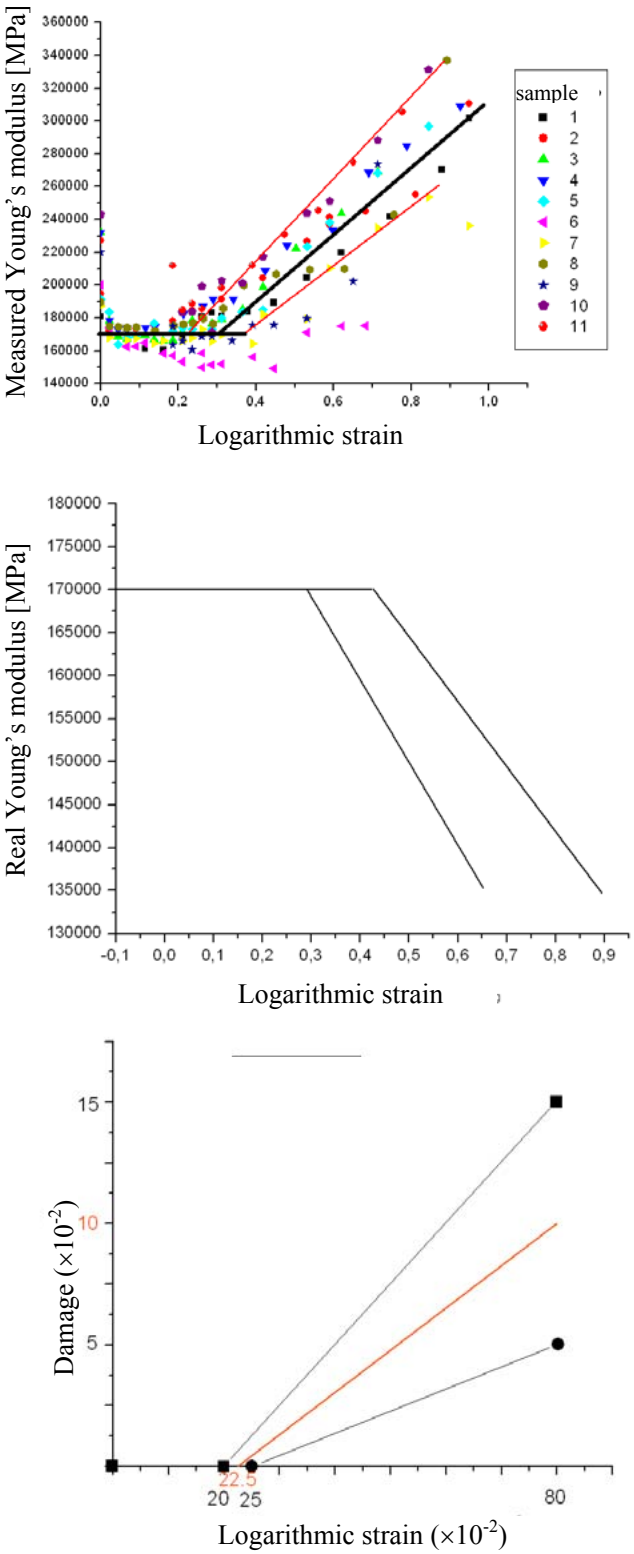

Figure 3: Damage characterization curves in terms of logarithmic strain for SAE 1020 steel. a) Measured uniaxial Young´s modulus, b) real Young's modulus and c) damage curve.

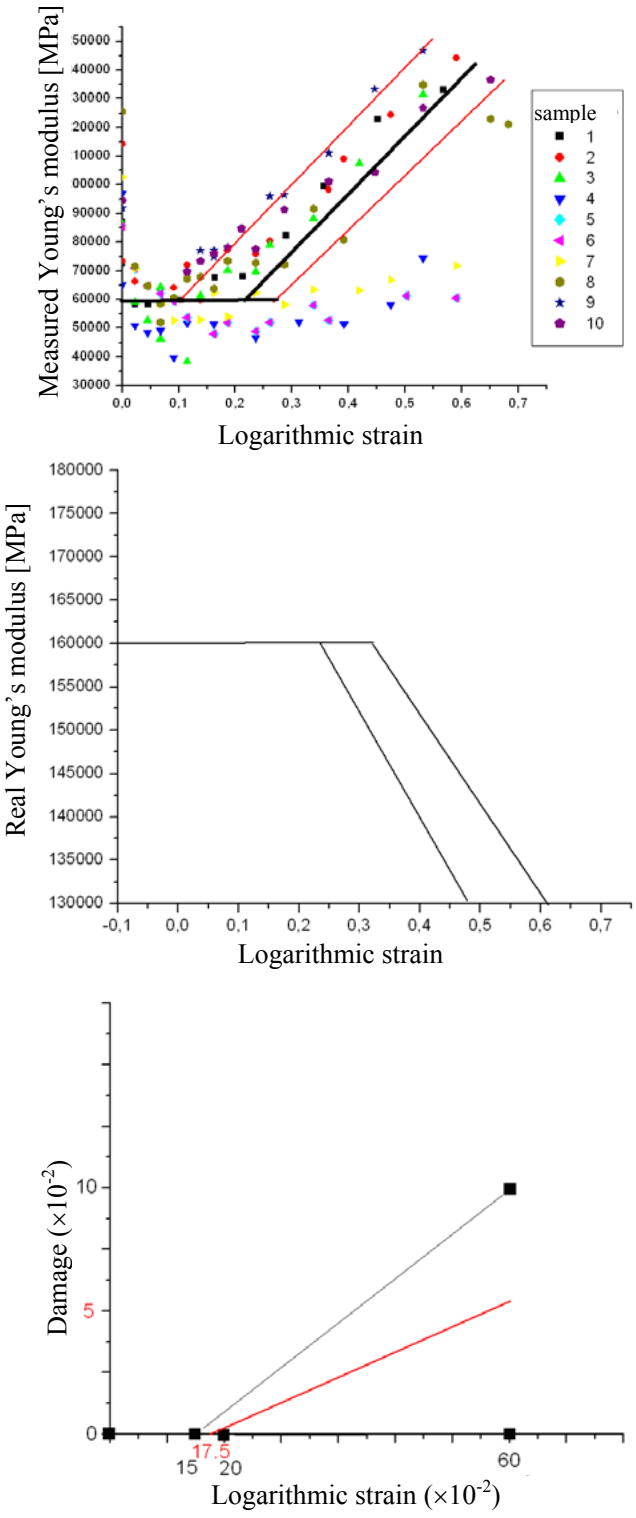

Figure 4: Damage characterization curves in terms of logarithmic strain for SAE 1045 steel. a) Measured uniaxial Young´s modulus, b) real Young's modulus and c) damage curve.

It should be noted that the definitions of $\psi=\psi(\mathbf{e},\alpha_k)$ and $D\alpha_k/Dt$ are crucial features of the model since they allow to derive all the constitutive equations presented above.

The internal variables and their corresponding evolution equations are defined in this work within a non-associate rate-independent plasticity theory context [15] including damage effects in a coupled form [1-12]. A possible choice is given by the plastic Almansi strain tensor $\mathbf{e}^p$, the effective plastic deformation $\bar{e}^p$ related to the isotropic strain hardening effect [1-15] and the damage variable d^p [1-12]. The evolution equations for such internal variables can be written as [1-13]:

$$L_v(\mathbf{e}^p) = \dot{\lambda}\,\partial F/\partial\boldsymbol{\tau} \qquad \dot{\bar{e}}^p = -\dot{\lambda}\,\partial F/\partial C^p \qquad \dot{d}^p = \dot{\lambda}\,\partial G/\partial Y^p \tag{8}$$

where $\boldsymbol{\tau}$ is the Kirchhoff stress tensor ($\boldsymbol{\tau}=J\boldsymbol{\sigma}$), L_v is the well-known Lie (frame-indifferent) derivative, $\dot{\lambda}$ is the rate (or increment in this context) of the plastic consistency parameter computed according to classical concepts of the plasticity theory [15], C^p is the plastic hardening function, Y^p is the conjugate variable of d^p (Y^p can be considered as the elastic strain energy release rate associated with a unit damage growth [5-9]) while $F(\boldsymbol{\sigma},\bar{e}^p,d^p)$ and $G(Y^p,d^p)$ are the flow potentials respectively related to purely plastic and damage effects accordingly related to plastic deformation and damage evolutions. In this context, F is also assumed as the yield function such that no plastic evolutions occur when $F<0$. Moreover, as stated by equation (8.c), note that a plasticity-driven damage phenomenon is adopted here which leads that no damage evolution is neither expected when $F<0$. A classical choice for metal plasticity is the Von Mises yield function:

$$F = \sqrt{3J_2} - C^p(1-d^p) \tag{9}$$

where J_2 is the second invariant of the deviatoric part of $\boldsymbol{\tau}$ and the plastic hardening function C^p is adopted in this work as [14]:

$$C^p = A^p(\bar{e}_0^p + \langle \bar{e}^p - \bar{e}_c^p \rangle)^{n^p} \tag{10}$$

where $\bar{e}_0^p$ is an assumed initial value of $\bar{e}^p$ such that $C^{th} = A^p \bar{e}_0^{p\ n^p}$ with C^{th} being the yield strength defining the initial material elastic bound. Moreover, $\langle\ \rangle$ are the Macauley brackets and $\bar{e}_c^p$ is a critical effective plastic strain accounting for the effect of Lüders´ band formation considered here as a perfectly plastic process, i.e., $\bar{e}_c^p$ is the maximum plastic deformation after the elastic response at which $C^p = C^{th}$ (if this phenomenon is not present, $\bar{e}_c^p = 0$ and the classical hardening expression $C^p = A^p(\bar{e}_0^p + \bar{e}^p)^{n^p}$ is recovered). The hardening material parameters A^p, n^p and $\bar{e}_c^p$ appearing in the isotropic strain hardening law (10) are assumed to characterize the material behavior in the plastic range (strain rates effects are neglected [14]). These parameters can be directly obtained through an experimental-based correlation [14].

Table 3 summarizes the average values of A^p, n^p and $\bar{e}_c^p$ for the two steels studied in this work. On the other hand, the expression adopted for G is [5-9]:

$$G = Y^{p\,2}\,\frac{d_r}{(\bar{e}_r - \bar{e}_d)}\,\frac{E(1-d^p)^2}{3J_2} \tag{11}$$

The following definition for the specific free energy function $\psi = \psi(\mathbf{e}-\mathbf{e}^p, \bar{e}^p, d^p)$ is considered:

$$\psi = \frac{1}{2\rho_0}(\mathbf{e}-\mathbf{e}^p):(1-d^p)\mathbf{C}:(\mathbf{e}-\mathbf{e}^p) + \frac{1}{\rho_0}(\mathbf{e}-\mathbf{e}^p):(1-d^p)\mathbf{C}:\boldsymbol{\tau}_0 + \frac{1}{(n^p+1)\rho_0}A^p(\bar{e}_0^p + \langle \bar{e}^p - \bar{e}_c^p \rangle)^{n^p+1} - \frac{1}{\rho_0}C^{th}\bar{e}^p + \psi_0 \tag{12}$$

where $\mathbf{C}$ is the isotropic elastic constitutive tensor. This last equation is a partially coupled form of defining ψ which can be considered nowadays well established since different versions of it have successfully been used in many engineering applications (see [14] and references therein). Moreover, the additive decomposition of the Almansi strain tensor is recovered in this context through the multiplicative decomposition of the deformation gradient into elastic and plastic contributions. In addition, note that, according to the definitions given above, the internal variables of this model together with their corresponding conjugates variables are $\boldsymbol{\alpha}_1 = \mathbf{e}^p$, $\alpha_2 = \bar{e}^p$, $\alpha_3 = d^p$ and $\boldsymbol{q}_1 = \boldsymbol{\tau}$, $q_2 = -(C^p - C^{th})$, $q_3 = Y^p$.

With these considerations, the stress-strain law (secant or hyperelastic form for the Cauchy stress tensor) and the expression of the internal dissipation are respectively given by:

$$\boldsymbol{\sigma} = \frac{1}{J}\left[(1-d^p)\mathbf{C}:(\mathbf{e}-\mathbf{e}^p) + \boldsymbol{\tau}_0\right] \tag{13}$$

$$D_{\text{int}} = \boldsymbol{\tau} : L_v(\mathbf{e}^p) - (C^p - C^{th})\dot{\bar{e}}^p - Y^p\dot{d}^p \geq 0 \tag{14}$$

where this last inequality is effectively fulfilled owing to the definitions adopted above.

4 SIMULATION AND EXPERIMENTAL VALIDATION

4.1 Tensile test

The performance of both the damage characterization and constitutive model respectively presented in Sections 2 and 3 are preliminary assessed in the simulation of the tensile test applied to the SAE 1020 and SAE 1045 steels.

The material parameters considered in the simulations are listed in Table 1.

Figure 5 shows the damage evolution at the point located at the center of the section that undergoes extreme necking at high levels of deformation. In accordance with the damage evolution (8.c) together with the damage potential definition given by equation (11), it is seen

that the damage variable starts at $\bar{e}_d$ and reaches it critical value d_c at $\bar{e}_r$. After this last deformation, the damage is assumed to grow in sudden way up to the condition $d_c=1$ that represents the macroscopic crack development. The final failure of the specimen takes place when all the points of this transversal area reach such limiting condition.

Some characteristic contour distributions developed at the neck for the fracture stage are presented in Figure 6. As expected, the effective plastic deformation evolves from the center to the edge of the sample. However, as a consequence of the high damage effects present in this zone, a significant reduction of the hardening function including damage $C^p(1-d^p)$ involved in the yield funtion (9) can be particularly appreciated at the center of the sample. Accordingly, the Von Mises stress also decreases in this region. Note that this trend exhibits a sharp contrast with that obtained in a simulation without accounting for damage evolution [14].

Table 1. Material parameters considered in the simulations.

Property	SAE 1020 steel	SAE 1045 steel
Young's modulus, E [MPa]	170000	160000
Poisson's ratio, ν	0.3	0.3
Yield strength, C^{th} [MPa]	333	450
Hardening coefficient, A^p [MPa]	731	1148
Hardening exponent, n^p	0.187	0.121
Critical effective pl. strain, $\bar{e}_c^p$	0.024	0.010
Strain at damage threshold, $\bar{e}_d$	0.225	0.175
Strain at failure, $\bar{e}_r$	0.800	0.600
Critical damage, d_r	0.10	0.05

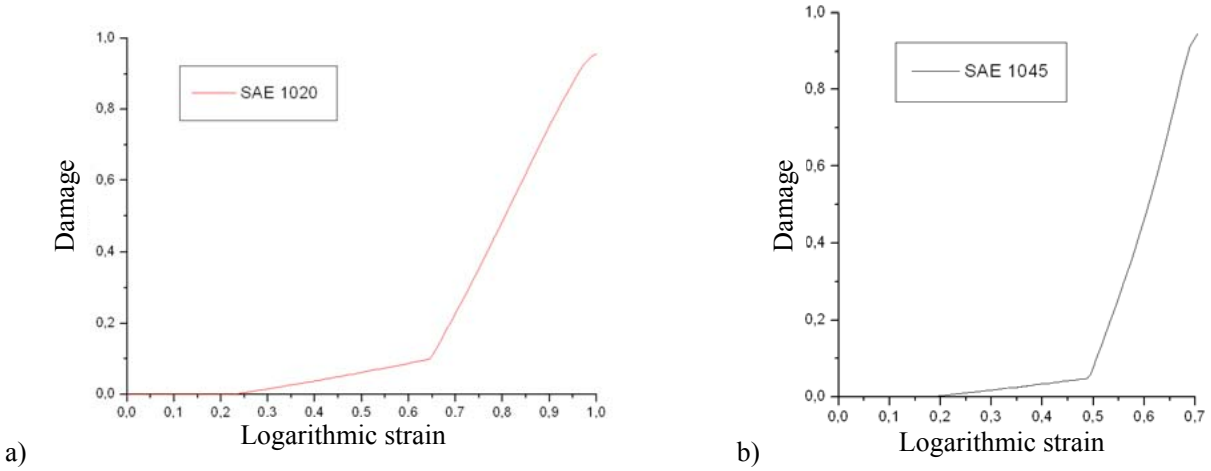

Figure 5: Simulation of the tensile test. Damage evolution for a) SAE 1020 and b) SAE 1045 steels at the center of the section undergoing extreme necking.

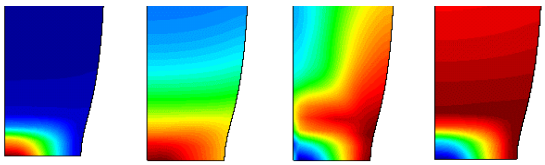

a) b) c) d)

Figure 6: Simulation of the tensile test. Characteristic contour distributions at the neck for the fracture stage: a) damage, b) effective plastic deformation, c) Von Mises stress and d) plastic hardening function including damage $C^p(1-d^p)$.

4.2 Flattening of a cylinder

As an application of the constitutive model briefly presented above including the damage parameters through the experimental characterization already described, the flattening process of a SAE 1020 steel cylinder is simulated. The aim of this analysis is to qualitatively compare the predicted material response with that observed in the experiments that were carried out by applying a compression force under displacement-controlled conditions.

a)

b)

Figure 7: Flattening of a cylinder. Final deformed configuration of the sample: a) general view and b) detail of the cracked zone.

The final geometric configurations of the samples tested are shown in Figure 7. A main macrocrack can be appreciated at the outer surface of the cylinder in the lateral zone where it experiences tensile stress and, consequently, larger stretchings. To what extent the model is able to simulate this effect is discussed below.

Once more, the material parameters used in the simulation are listed in Table 1.

Figure 8 shows contour distributions of $\bar{e}^p$ and d^p at the end of the process. A detail of the contour distributions of the damage variable and the pressure to Von Mises ratio I_1/J_2 ($I_1=1/3tr(\boldsymbol{\sigma})$, where tr is the trace symbol) is plotted in Figure 9. It is seen that the corresponding larger values of these variables are located at the inner part of the cylinder. Consequently, this is the region where the model predicts the macrocrack location. This part, however, is mainly subjected to compression and, therefore, a visible crack does not occur there during the experimental tests. In contrast this, the outer region undergoes tensile stress with damage values near to d_c which is, in fact, the onset of macrocrack formation [5-9]. Note that this is a limiting aspect of the model due to the isotropic damage evolution assumed in it.

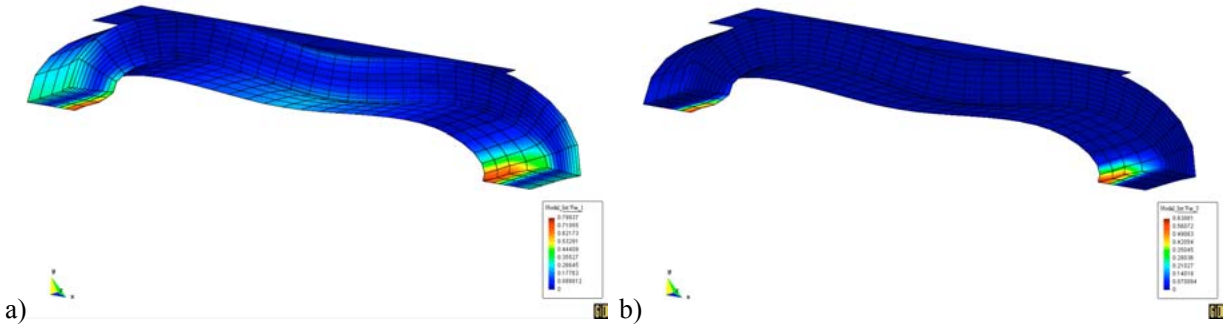

Figure 8: Simulation of the flattening of a cylinder. Contour distributions at the end of the process: a) effective plastic deformation and b) damage.

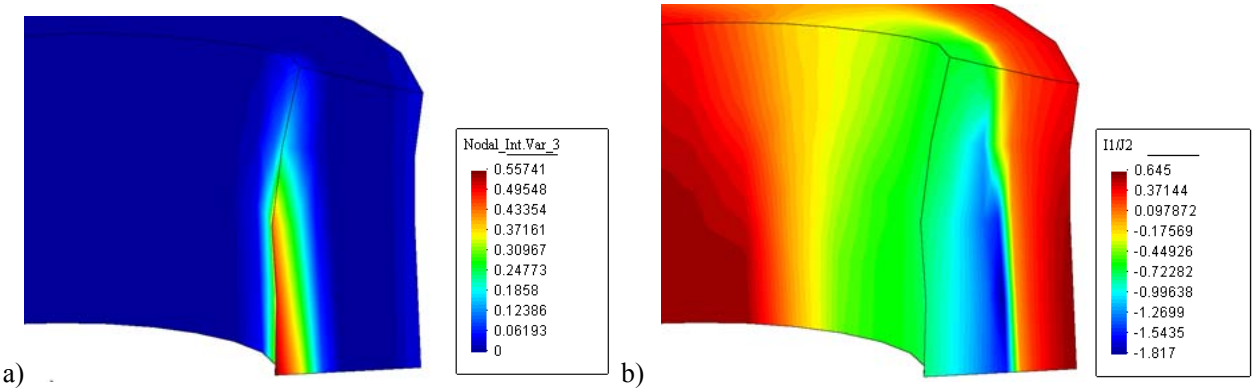

Figure 9: Simulation of the flattening of a cylinder. Detail of contour distributions at the end of the process: a) damage and b) pressure to Von Mises stress ratio I_1/J_2.

5 CONCLUSIONS

An experimental and numerical characterization of the ductile damage evolution that takes place in loaded steels has been presented. Some relevant details about this procedure have been discussed. The material parameters derived from it have been used in the numerical analysis of two deformation processes: the tensile test and the flattening of a cylinder. It was observed that the isotropic damage model adopted for these analyses can cope with monotonic tensile loading but, in contrast, is not able to realistically deal with compression stress states. Some modifications related with this aspect will be explored in future works.

6 ACKNOWLEDGEMENTS

The support provided by the Chilean Council of Research and Technology CONICYT (FONDECYT Projects Nos. 1020026 and 7020026) and the Department of Technological and Scientific Research at the University of Santiago de Chile (DICYT-USACH) are gratefully acknowledged. The authors wish to express their appreciation to the Laboratory of Mechanical Testing belonging to the Department of Metallurgical Engineering at USACH for the provision of experimental facilities.

7 REFERENCES

[1] J. Hult, “Continuum Damage Mechanics - Capabilities, limitations and promises”, in Mechanisms of Deformation and Fracture, Pergamon, Oxford, pp. 233-347 (1990).

[2] J. L. Chaboche, “Continuous Damage Mechanics : a tool to describe phenomena before crack initiation”, Nuclear Engineering and Design, Vol.64, pp.233-247 (1981).

[3] S. Murakami, “Notion of Continuum Damage Mechanics and its application to anisotropic creep damage theory”, J. Eng. Mat. and Technology, Vol. 105, p. 99 (1983).

[4] D. Krajcinovic, “Continuum Damage Mechanics”, Applied Mechanics Reviews, Vol. 37, pp. 1-6 (1984).

[5] J. Lemaitre, “A continuous damage mechanics model for ductile fracture”, Journal of *Engineering Materials and Technology*, 107, 83-89 (1985).

[6] J. Lemaitre, “Coupled elasto plasticity and damage constitutive equations”, *Computer Methods in Applied Mechanics and Engineering*, 51, 31-49 (1985).

[7] J. Lemaitre and J. Dufailly, “Damage measurements”, *Engineering Fracture Mechanics*, 28, 643-661 (1987).

[8] J. L. Chaboche, “Continuum damage mechanics: Part I – General concepts”, *Journal of Applied Mechanics*, 55, 59-64 (1988).

[9] J. L. Chaboche, “Continuum damage mechanics: Part II – Damage growth, crack initiation, and crack growth”, *Journal of Applied Mechanics*, 55, 65-72 (1988).

[10] B. Luccioni, S. Oller and R. Danesi, “Coupled plastic-damaged model”, *Computer Methods in Applied Mechanics and Engineering*, 129, 81-89 (1996).

[11] F. Armero and S. Oller, “A general framework for continuum damage models. I.

Infinitesimal plastic damage models in stress space", *International Journal of Solids and Structures*, 37, 7409-7436 (2000).

[12] F. Armero and S. Oller, "A general framework for continuum damage models. II. Integration algorithms, with applications to the numerical simulation of porous metals", *International Journal of Solids and Structures*, 37, 7437-7464 (2000).

[13] P. Tapia, "Experimental and numerical characterization of damage evolution in steels", Master Thesis (in Spanish), Universidad de Santiago de Chile (2004).

[14] E. Cabezas and D. Celentano, "Experimental and numerical analysis of the tensile test using sheet specimens", *Finite Elements in Analysis and Design*, 40, 555-575 (2004).

[15] J. Lubliner, *Plasticity Theory*, Macmillan Publishing, New York (1990).